Arch. Metall. Mater. **64** (2019), 3, 883-888

DOI: 10.24425/amm.2019.129466

SANG WOO LEE*, HYUNHO SHIN**#, KYONG YOP RHEE*#

DENSIFICATION AND MECHANICAL PROPERTIES OF 439L STEEL COMPOSITES BLENDED WITH FIFTEEN MICRON-SIZE SILICON CARBIDE PARTICLES

439L stainless steel composites blended with fifteen micron SiC particles were prepared by uniaxial pressing of raw powders at 100 MPa and conventional sintering at 1350°C for 2 h. Based on the results of X-ray diffraction analysis, dissolution of SiC particles were apparent. The 5 vol% SiC specimen demonstrated maximal densification (91.5%) among prepared specimens (0-10 vol% SiC); the relative density was higher than the specimens in the literature (80-84%) prepared by a similar process but at a higher forming pressure (700 MPa). The stress-strain curve and yield strength were also maximal at the 5 vol% of SiC, indicating that densification is the most important parameter determining the mechanical property. The added SiC particles in this study did not serve as the reinforcement phase for the 439L steel matrix but as a liquid-phase-sintering agent for facilitating densification, which eventually improved the mechanical property of the sintered product.

Keywords: 439L steel, silicon carbide, composites, densification, liquid-phase sintering

1. Introduction

Powder metallurgy-processed metal matrix composites (MMCs) blended with refractory particle phases such as silicon carbide have received much interest for applications to automotive compartments. Because the powder metallurgy process resorts to sintering of particles for densification of powder compact, presence of pores in the sintered body is inevitable, which limits the full manifestation of the mechanical properties of fabricated composites. In spite of the presence of pores, the powder metallurgy-processed MMCs draws interest because of cost efficiency. This study focuses on the SiC particle-added steel matrix composites.

Employing a fine particle size of the refractory phase (SiC) and non-conventional sintering process such as the spark plasma sintering [1-2] and hot isostatic pressing [3-4] process is beneficial in promoting densification with steel matrix, while the fine particle sizes and non-conventional sintering processes impose the burden in cost. In the literature [1-4], majority of studies employed fine SiC particles (1-10 μm) or the non-conventional sintering processes. The studies which employed the conventional sintering process were relatively sparse [5-7]. In such a case, the forming pressure of the powder compact blended with fine SiC particles was as high as 700 MPa and the relative density of the sintered composites was in the range 76-80%, while mechanical properties such as the stress-strain curve of the composites were hardly reported.

If a study on the low cost processing which employs the conventional sintering process, a larger SiC particles, and a lower forming pressure of the powder compact is carried out, it would facilitate manifestation of steel matrix composites blended with SiC particles for engineering compartments. The characterization of not only the densification of the prepared composites but also the mechanical property such as the simple compressive-stress-strain curve may contribute to comparing the performance of the prepared composites with those of future studies. In these regards, this study employs the conventional sintering process, an average particle size of SiC of 15 μm, and a forming pressure of 100 MPa, which should impose a mild burden in cost. Under such constraints, this study (i) investigates whether the addition of a 15 μm SiC powder can improve densification compared with the reference steel powder itself, (ii) uncovers the associated mechanism for the improved densification (in terms of crystal phases and dissolution of SiC), and (iii) characterizes the level of the achieved relative density and mechanical property of the sintered composites in terms of the compressive stress-strain curve.

2. Experimental

The average particle size of the 439 L stainless steel powder used in this study was 41 μm (Daeshin Co., Ulsan, Korea). Its manufacturer-provided composition is: Cr: 18 at%, Si: 0.75 at%, Mn 0.5 at%, Ni: 0.5 at%, C: 0.025 at% with balanced Fe. The average particle size of the SiC powder used in this study was 15 μm (F-800, Kumthai Abrasives Co., Ltd, Zhengzhou, China).

* KYUNGHEE UNIVERSITY, DEPARTMENT OF MECHANICAL ENGINEERING, YONGIN, GYOENGGI-DO 17104, REPUBLIC OF KOREA
** GANGNEUNG-WONJU NATIONAL UNIVERSITY, DEPARTMENT OF MATERIALS ENGINEERING, GANGNEUNG, GANGWON-DO 25457, REPUBLIC OF KOREA
# Corresponding authors: hshin@gwnu.ac.kr, rheeky@khu.ac.kr

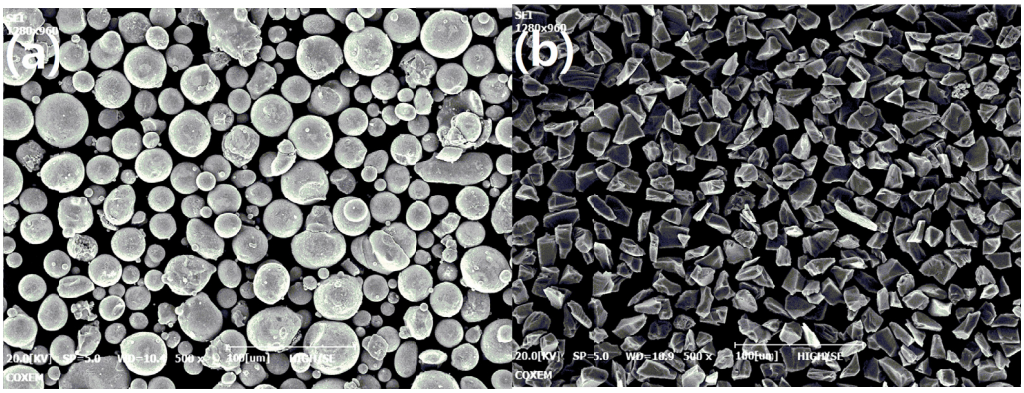

Fig. 1. Morphology of the particles used in this study. (a) 439 L steel and (b) SiC powders

Its manufacturer-provided composition is: SiC ≥ 97.00 wt.%, F and C: 0.35 ≤ wt.%, Fe_2O_3 ≤ 0.50 wt.%. Morphologies of the 439 L steel and SiC powders are presented in Fig. 1.

The steel powder, SiC powder, and stearic acid lubricating agent (Daejung Chemical Co., Siheung, Korea) were dry-mixed in a rolling glass bottle for 60 min. The volume percentages of SiC powder in the SiC-steel system were 0, 1, 3, 5, and 10 vol%. The amount of the stearic acid was 1.2 wt.% in the SiC-steel-stearic acid system. An aliquot of ethanol was added to the mixed powder, followed by uniaxial pressing in a stainless steel mold with a diameter of 15 mm at 100 MPa. The pressed body was transferred to an alumina tube furnace and sintered at 1350°C (heating speed of 7°C/min) for 2 h in a flowing N_2-10%H_2 atmosphere.

The sintered body was machined to a cylinder with a diameter of 6 mm and height of 6 mm. The apparent density of the machined specimen was measured via the Archimedes principle. The top surface of the cylinder specimen was polished using the diamond paste (6 and 3 μm) for microstructural observation via scanning electron microscopy (SEM) and electron probe microanalysis (EPMA). Microstructural images in secondary electron (SE) and backscattered electron (BSE) modes were taken together with area analysis for Si.

The machined cylinder specimen was subjected to the compression test using the universal tester with a 10 ton load cell. An aliquot of nano-WS_2-silicone oil mixture was applied as the lubricant between the top/bottom surface of the cylinder and the tungsten carbide (with 6 mol% cobalt) platen. The loading direction of the cylinder specimen was the same as the pressing direction of the powder compact in the mold in the processing stage. The nominal strain rate for the compression test was 3×10^{-3} s^{-1} and the test was carried out at ambient temperature. The measured load-displacement curve was converted to the curve of true stress-strain by assuming volume constancy of the specimen; the compressible nature of the specimen due to the presence of pores was neglected in the conversion process.

After the compression test, the tested specimen was pulverized using mortar and pestle, both made of alumina, followed by cryogenic milling to obtain particles that can pass 75 μm sieve (200 mesh). The pulverized specimen was subjected to X-ray diffraction (XRD) analysis for the identification of crystal phases.

3. Results and discussion

3.1. Identification of crystalline phases

Crystal phases of the sintered composites, identified via XRD analysis, are presented in Fig. 2. As can be observed in Fig. 2, only the iron peaks (marked as #) are identified up to the composition with 10 vol% SiC. The absence of SiC peaks in the XRD pattern does not guarantee that there is no SiC phase in the specimen but the absence of SiC peaks in the 10 vol% SiC specimen clearly indicate that the dissolution of the SiC particles in the 439L steel matrix is significant, which is possible via the formation of a Fe-SiC eutectic liquid phase.

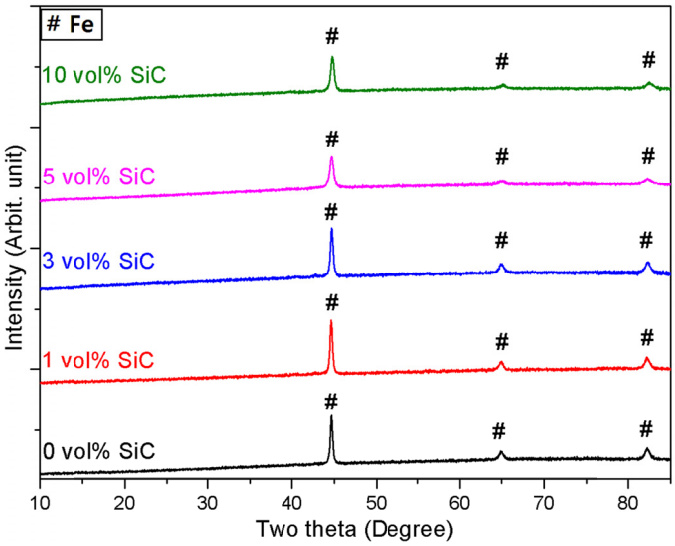

Fig. 2. XRD patterns of the prepared composites

In the literature [8-13], the high-temperature reaction of SiC with steel powder resulted in various crystal phases such as Fe-SiC, Fe-Si, Fe_3Si, M_7C_3, and Fe_2Si. In this study (Fig. 2), however, no such phases are found although dissolution of SiC was significant. In general, it is difficult to achieve perfectly pure SiC particles because SiC particles are generally obtained via the process of pulverization of a lager SiC chunks prepared by carbothermal reduction of SiO_2; impurities can be included

suitably in the pulverization process. The difference in chemical composition (impurities) and the processing route of the composites are believed to be ascribed to the difference in the observed crystal phase between this study and existing ones [8-13].

3.2. Microstructural identification of the silicon-rich area

As no appreciable SiC peaks were identified in the XRD pattern (Fig. 2), microstructural identification of the silicon-rich area was pursued via EPMA analysis. The results are shown in Figs. 3-6. Frame (e)'s of these figures present the average level of Si area percent in a 0-400 scale; it increases from 11 to 37 as the concentration of SiC increases from 1 to 10 vol%. In the 1 vol% SiC specimen (Fig. 3), the size of the silicon-rich red spots is only a couple of microns at best, which is much smaller than the initial size of the SiC particles (15 μm). These red spots and blue areas may be residual SiC particles survived from dissolution but were not identified in XRD analysis due to the small quantity or be the silicon-rich amorphous phase.

In the 3 vol% SiC specimen (Fig. 4), the red spots almost disappear, which is possibly because the concentration of the Si element was more homogenized in this specimen due to the enhanced formation of the SiC-dissolved liquid phase. Note that

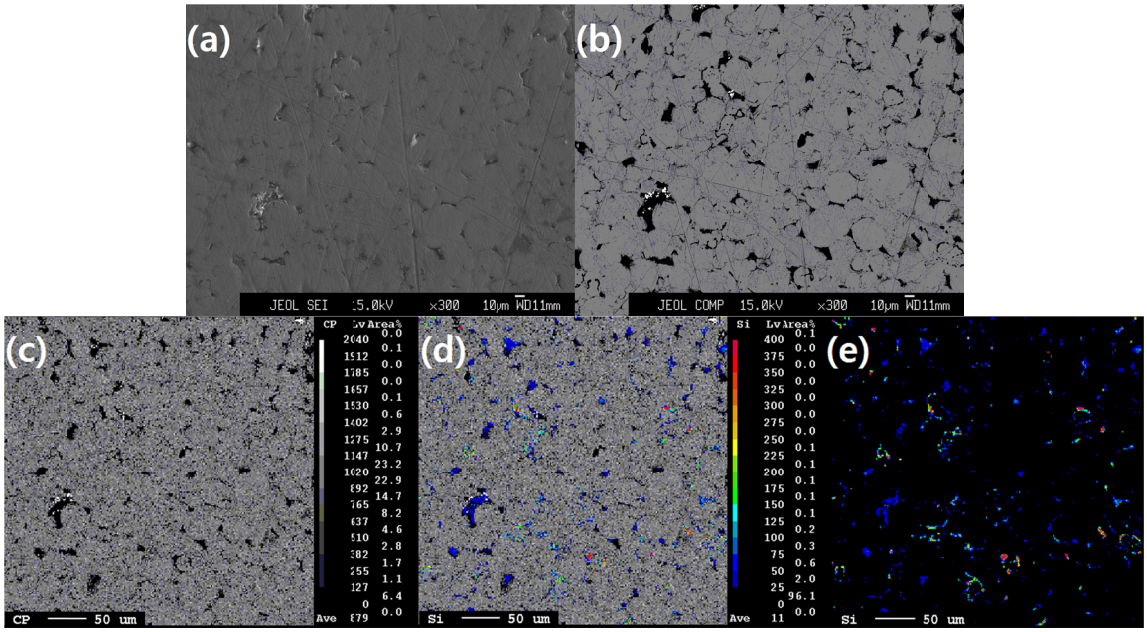

Fig. 3. EPMA analysis results for the specimen with 1 vol% SiC. (a) SE- and (b) BSE-mode images. (c) The BSE-mode image for area analysis of Si. (d) Superimposed images of (c) and (e). (e) The area analysis result for Si

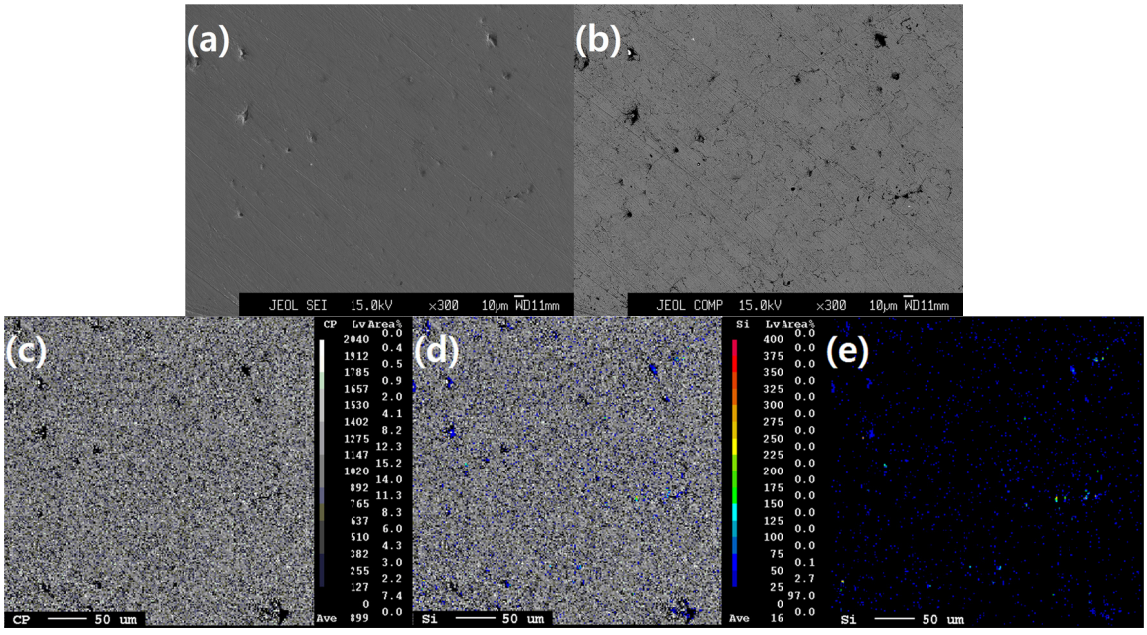

Fig. 4. EPMA analysis results for the specimen with 3 vol% SiC. (a) SE- and (b) BSE-mode images. (c) The BSE-mode image for area analysis of Si. (d) Superimposed images of (c) and (e). (e) The area analysis result for Si

the average level of the Si area percent increased from 11 to 16 as the SiC concentration increased from 1 to 3 vol%.

In the 5-10 vol% SiC specimens (Fig. 5-6), the size of some red spots is now comparable to the initial size. Even though these large red spots are the residual SiC particles survived from dissolution, they may not be detected in XRD analysis due to their small quantity.

Another important point in frame (b)'s of Figs. 5-6 is that the grain size (approximately 150 μm) has increased drastically from the specimens with 1-3 vol% SiC (approximately 44 μm). The larger amount of SiC-dissolved liquid phase at these compositions than the specimens with 1-3 vol% SiC is believed to foster the grain growth but uncovering further detailed mechanism for such a drastic grain growth process at 5-10 vol% SiC specimens needs further study.

Finally note in Fig. 5(b)-5(d) that the matrix region near the grain boundary is relatively darker than the interior; the core-shell structure of the grain is observed in Fig. 5(b)-5(d) but not in Figs. 6(b)-6(d). The darker shell area in Fig. 5(b) results from the higher concentration of light elements such as Si and C compared with Fe. In the 10 vol% SiC specimen (Fig. 6(b)), sufficient amounts of Si and C in the liquid phase at the grain boundary might have resulted in their suitable diffusion up to the interior region. In the 5 vol% SiC specimen (Fig. 5(b)), however,

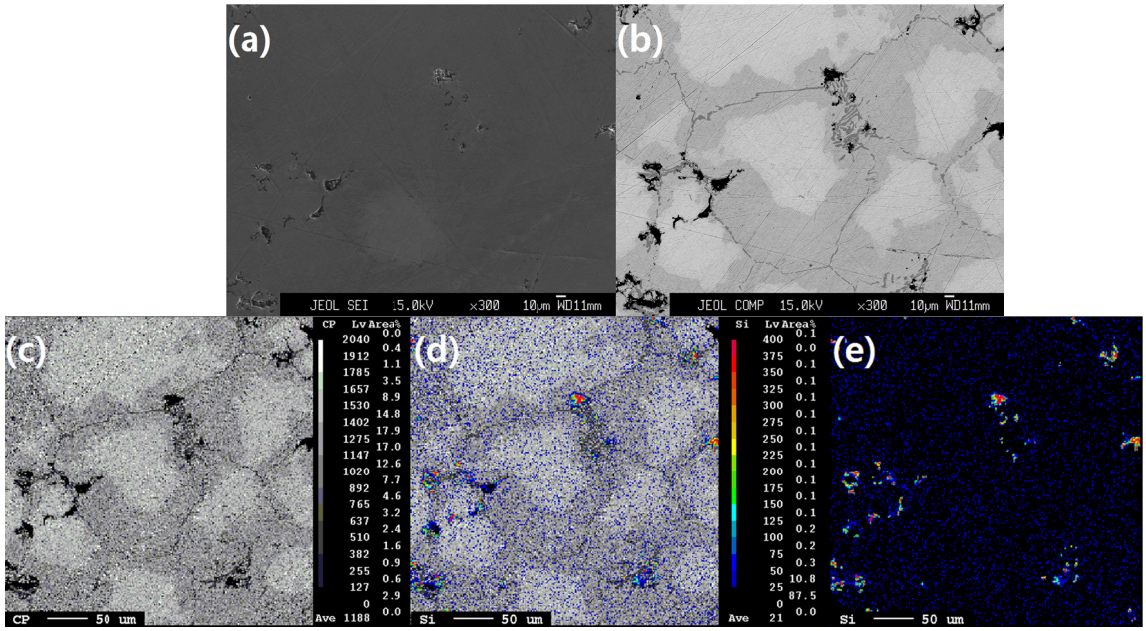

Fig. 5. EPMA analysis results for the specimen with 5 vol% SiC. (a) SE- and (b) BSE-mode images. (c) The BSE-mode image for area analysis of Si. (d) Superimposed images of (c) and (e). (e) The area analysis result for Si

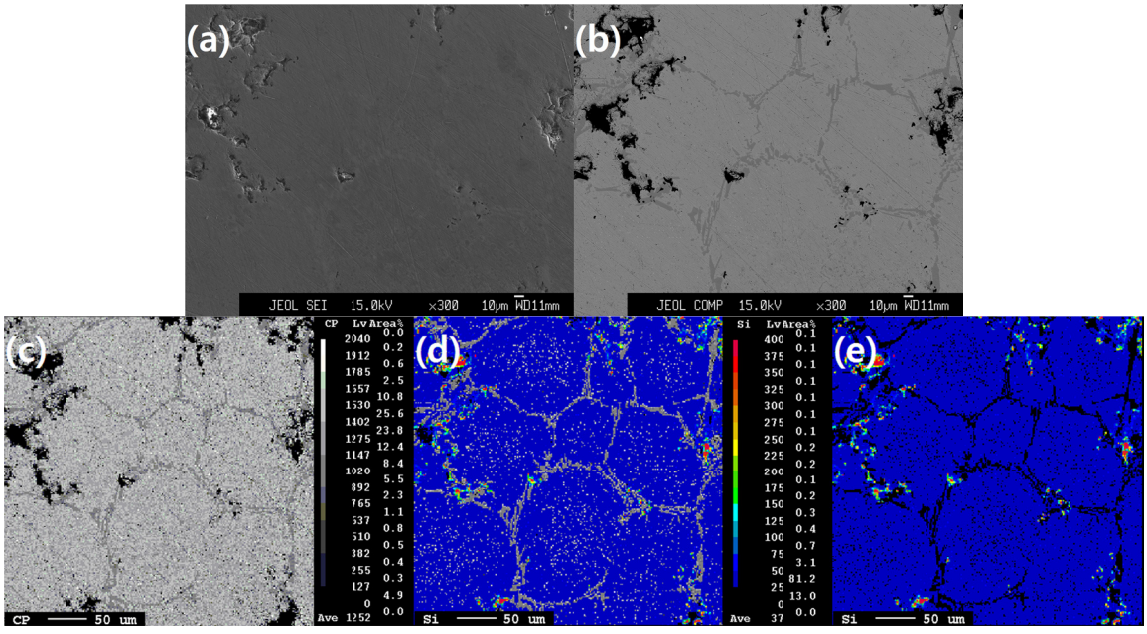

Fig. 6. EPMA analysis results for the specimen with 10 vol% SiC. (a) SE- and (b) BSE-mode images. (c) The BSE-mode image for area analysis of Si. (d) Superimposed images of (c) and (e). (e) The area analysis result for Si

available Si and C in the form of the liquid phase is relatively limited so their diffusion might have been achieved only up to a limited distance from the grain boundary. The diffusion of light elements into the 439L grain at 1-3 vol% SiC specimens where the drastic grain growth is limited needs further investigation.

3.3. Densification and mechanical property

To check the densification of the sintered composites, their microstructure was investigated at a much lower magnification than in Figs 3-6. The result is shown in Fig. 7. The pits in the dark color in Fig. 7 indicate pores. The total volume of pores are markedly diminished at the composition of 5 vol% SiC. This observation is consistent with the measured result of the relative density that will be shown later in Fig. 8(a).

The relative density, compressive stress-strain curve, and yield strength of the prepared composites are presented in Fig. 8. As mentioned, the relative density is maximal at the 5 vol% SiC specimen (Fig. 8(a)) among the prepared specimens (0-10 vol% SiC). Two reasons can be conceived of for the maximal densification at the 5 vol% SiC specimen. First, the composition and amount of the eutectic melt formed at the 5 vol% SiC specimen may be the most suitable for grain boundary wetting and densification of 439L steel grains. Second, the little amount of survived SiC phase (although not detected in XRD) from dissolution may increase in the 10 vol% SiC specimen, which may introduce its refractory nature to the specimen to hinder densification at an overly high concentration of SiC.

The stress-strain curve (Fig. 8(b)) and the yield strength (Fig. 8(c)) are also maximal at the 5 vol% of SiC, indicating that densification is the most important parameter determining the mechanical property. When the conventional sintering process was employed in the literature [5-7] with a higher forming pressure of 700 MPa than this study (100 MPa), the relative density of the SiC-steel composites was 80-84%. This study (Fig. 8(a)) achieves higher relative density (91.5%) than these references, resulting from enhanced liquid phase sintering possibly due to the difference in sintering temperature, particle size, and composition (impurity) of SiC and steel particles from those in existing studies. In this study, the added SiC particles did not serve as the reinforcement phase for the 439L steel matrix but as a liquid-phase-sintering agent for facilitating densification of the steel matrix, which eventually improved the mechanical property of the sintered body.

4. Conclusions

439L stainless steel composites blended with 15 micron SiC particles were prepared by uniaxially pressing raw powders at 100 MPa and conventionally sintering at 1350°C for 2 h. Based on the results of X-ray diffraction analysis, dissolution of SiC particles was apparent; no other crystalline phases than the crystal phase of iron were observed. The size of 439L steel grain was more or less similar to the initial size of the raw powder (44 μm) in 1-3 vol% SiC specimens while the size increased drastically to approximately 150 μm in 5-10 vol% SiC specimens. The 5 vol% SiC specimen demonstrated maximal densification (91.5%)

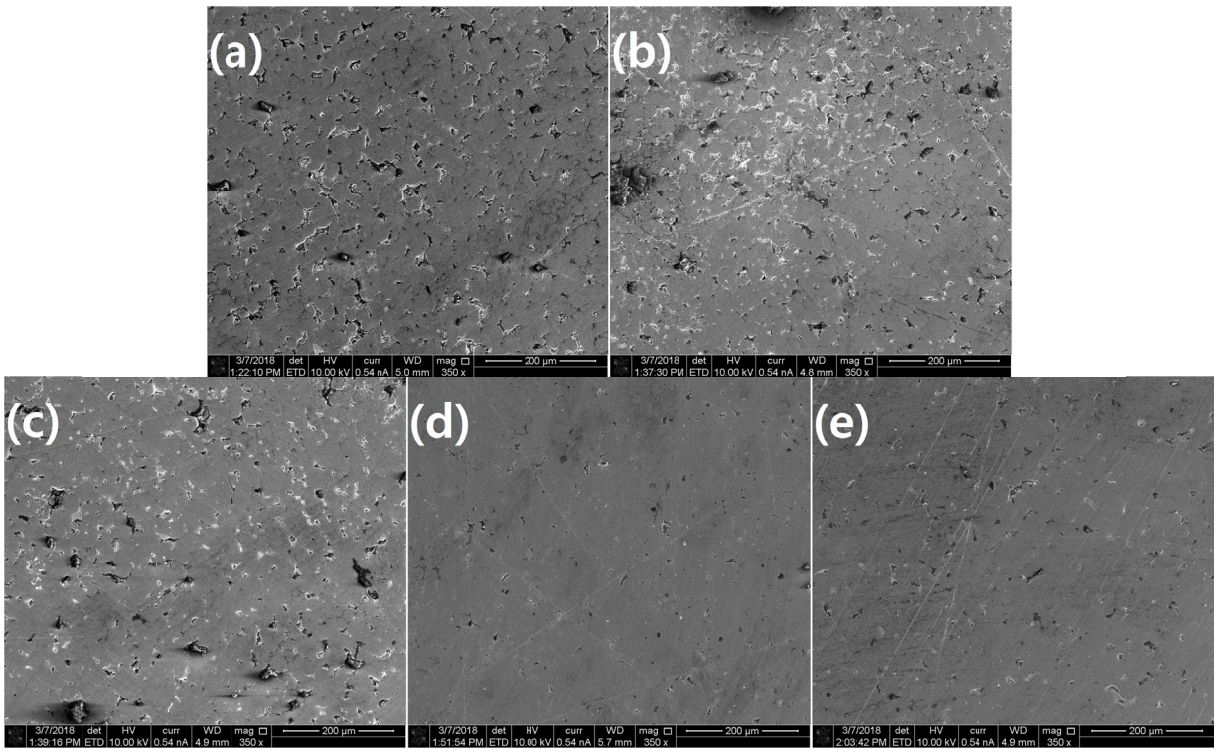

Fig. 7. Microstructures of the sintered composites observed via the SE-mode scanning electron microscopy. The compositions of specimens are (a) 0, (b) 1, (c) 3, (d) 5, and (e) 10 vol% SiC

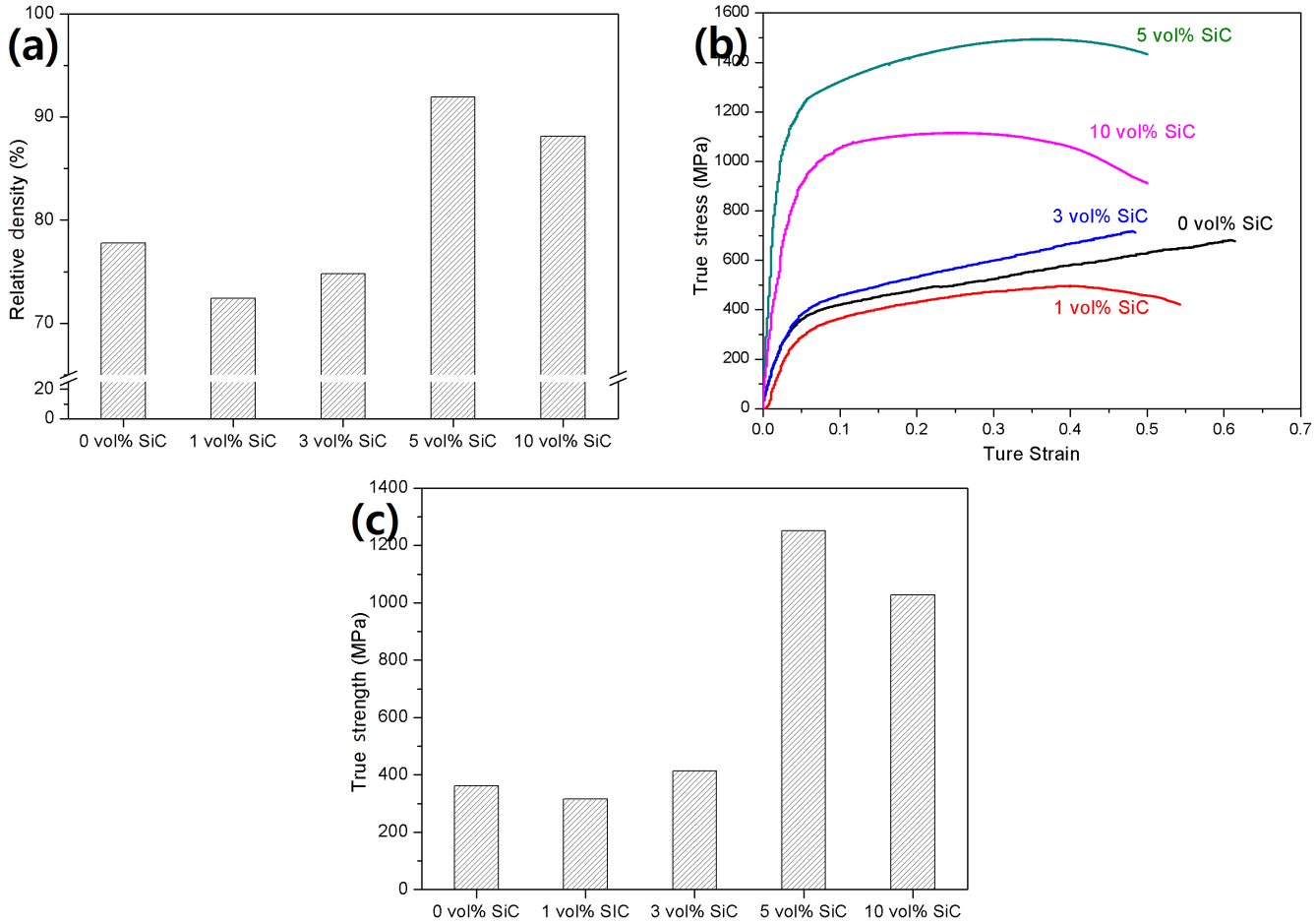

Fig. 8. (a) Relative density, (b) stress-strain curve, and (c) yield strength of the prepared composites

among prepared specimens (0-10 vol% SiC). This degree of densification was higher than the specimens in the literature (80-84%) which employed the same conventional powder metallurgy process as this study but a higher forming pressure of 700 MPa. The stress-strain curve and the yield strength were also maximal at the 5 vol% of SiC specimen, indicating that densification is the most important parameter determining the mechanical property. The added SiC particles in this study did not serve as the reinforcement phase for the 439L steel matrix but as a liquid-phase-sintering agent for facilitating densification of the matrix, which eventually improved the mechanical property of the sintered product. The relative density and the compressive yield strength of the specimen with a 5 vol% SiC were 118.1 and 346.0%, respectively, with reference to the sintered 439L steel without SiC.

Acknowledgments

This research was supported by the Ministry of Trade, Industry & Energy (MOTIE), Korea Institute for Advancement of Technology(KIAT) and Ulsan Institute For Regional Program Evaluation(IRPE) through the Encouragement Program for The Industries of Economic Cooperation Region.

REFERENCES

[1] C. Binder, T. Bendo, R.V. Pereira, G. Hammes, J.D.B. de Mello, A.N. Klein, Powder Metall. **59**, 384-393 (2016).
[2] Z. Hu, K. Ning, K. Lu, Mater. Sci. Eng. A-Struct. **A670**, 75-80 (2016).
[3] S.N. Patankar, M. Chnadrasekaran, M.J. Tan, J. Mater. Sci. Lett. **19**, 613-615 (2000).
[4] S.N. Parankar, M.J. Tan, Powder Metall. **43**, 350 (2000).
[5] J. Abenojar, F. Velasco, J.M. Torralba, J.A. Bas, J.A. Calero, R. Marce, Mater. Sci. Eng. A-Struct. **A335**, 1-5 (2002).
[6] J. Abenojar, F. Velasco, A. Bautista, M. Campos, J.A. Bas, J.M. Torralba, Compos. Sci. Technol. **63**, 69-79 (2003).
[7] O. Ertugrul, H.-S. Park, K. Onel, M, Willert-Porada, Powder Metall. **58**, 41-50 (2014).
[8] R.C.J. Schiepers, F.J.J. Loo, G. With, J. Am. Ceram. Soc. **71**, 284-287 (1988).
[9] T.C. Chou, A. Joshi, J. Am. Ceram. Soc. 74, 1364-1372 (1991).
[10] W.M. Tang, Z.X. Zheng, H.F. Ding, Z.H. Jin, Mater. Chem. Phys. 80, 360-365 (2003).
[11] S. Buytoz, M.M. Yildirim, H. Eren, Mater. Lett. **59**, 607-614 (2005).
[12] S. Buytoz, Surf. Coat. Technol. **200**, 3734-3742 (2006).
[13] J.D. Majumdar, B.R. Chandra, A.K. Nath, I. Manna, J. Mater. Process. Technol. **203**, 505-512 (2008).